HHS Public Access

Author manuscript

Curr Biol. Author manuscript; available in PMC 2020 February 18.

Published in final edited form as:

Curr Biol. 2019 February 18; 29(4): 554–566.e4. doi:10.1016/j.cub.2019.01.009.

Neural substrates of *Drosophila* larval anemotaxis

Tihana Jovanic[1,*,#], **Michael Winding**[1], **Albert Cardona**[1], **James W. Truman**[1,2], **Marc Gershow**[3,4,5,*], and **Marta Zlatic**[1,*]

[1]Janelia Research Campus, Howard Hughes Medical Institute, 19700 Helix drive, Ashburn, VA, 20147

[2]Friday Harbor Laboratories, University of Washington, Friday Harbor, WA 98250, USA.

[3]Department of Physics, New York University, New York, USA

[4]Center for Neural Science, New York University, New York, USA

[5]Neuroscience Institute, New York University, New York, USA

Summary

Animals use sensory information to move towards more favorable conditions. *Drosophila* larvae can move up or down gradients of odors (chemotax), light (phototax), and temperature (thermotax) by modulating the probability, direction, and size of turns based on sensory input. Whether larvae can anemotax in gradients of mechanosensory cues is unknown. Further, while many of the sensory neurons that mediate taxis have been described, the central circuits are not well understood. Here we used high-throughput, quantitative behavioral assays to demonstrate *Drosophila* larvae anemotax in gradients of wind speeds and to characterize the behavioral strategies involved. We found that larvae modulate the probability, direction and size of turns to move away from higher wind speeds. This suggests similar central decision-making mechanisms underlie taxis in somatosensory and other sensory modalities. By silencing the activity of single or very few neuron types in a behavioral screen, we found two sensory (chordotonal and multidendritic class III) and six nerve cord neuron types involved in anemotaxis. We reconstructed the identified neurons in an electron microscopy volume that spans the entire larval nervous system and found they received direct input from the mechanosensory neurons or from each other. In this way we identified local interneurons, and first- and second-order SEZ and brain projection neurons. Finally, silencing a dopaminergic brain neuron type impairs anemotaxis. These findings

[*]Correspondence: **Tihana Jovanic** – jovanict@janelia.hhmi.org.
Present address: Paris-Saclay Institute of Neuroscience, UMR 9717, 1, avenue de la Terrasse, 91190, Gif-sur-Yvette, tihana.jovanic@cnrs.fr, Decision and Bayesian computation, Institut Pasteur, 75015 Paris, France, **Marc Gershow** – marc.gershow@nyu.edu, **Marta Zlatic** –zlaticm@janelia.hhmi.org

Author Contributions

T.J., M.G. and M.Z. conceived the project, T.J. performed the experiments, T.J and M.G analyzed the data, M.G. provided the analysis software, M.W. performed EM reconstructions, J.W.T provided reagents, A.C. provided unpublished data and expertise on EM reconstruction of neuronal connectivity T.J. and M.Z wrote the manuscript

[#]Lead contact

Declaration of Interests

The authors declare no competing interest.

suggest anemotaxis involves both nerve cord and brain circuits. The candidate neurons and circuitry identified in our study provide a basis for future detailed mechanistic understanding of the circuit principles of anemotaxis.

eTOC Blurb

Jovanic et al. use high-throughput quantitative behavioral analysis, manipulation of neuronal activity and EM reconstruction of neuronal connectivity to characterize *Drosophila* larva anemotactic behavior and identify two types of sensory neurons, six nerve cord neurons and a brain dopaminergic neuron cluster all implicated in anemotaxis.

Graphical Abstract

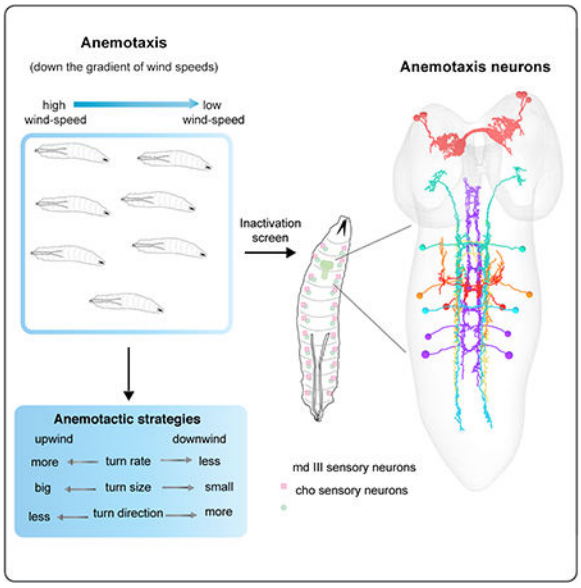

Keywords

anemotaxis; neural substrates; *Drosophila* larva; CNS; somatosensory processing

Introduction

Many animals have been shown to be capable of sensing air-currents and moving with respect to the direction and speed of the wind. In nature wind can carry information about appetitive or aversive odors. Also predators may generate air disturbances that can be detected by the preys [1]. Thus being able to orient one's movement with respect to the direction of the wind may allow animals to find food or to avoid dangers [2–5]. In addition, information about the wind direction can be used by animals with limited perceptual range to make movement decisions (i.e. to keep straight course) during search behaviors [6]. The ability to move up or down air-current gradients may therefore be shared and important for survival across the animal kingdom from invertebrate species to mammals. This behavior is called anemotaxis (from the Greek *anemo* - άνεμο for wind and taxis - τάξις for

arrangement). Animals can perform both positive and negative anemotaxis, depending whether they move upwind or downwind [2–5, 7].

While some sensory hairs and hair like organs that mediate anemotaxis in multiple species have been identified [8–11] the neural underpinnings of how information about the wind direction is transformed into directional behavioral responses during anemotaxis in the central nervous system have been understudied.

Small genetic model organisms like *Drosophila* larva are well suited for discovering circuit implementation of taxis strategies in sensory gradients by combining targeted neuronal manipulations with high-throughput behavioral assays and electron microscopy reconstruction of neural circuits.

Larvae have been shown to perform taxis in gradients of odors, CO_2, light and temperature and the computations and the behavioral dynamics of taxis behaviors in these sensory gradients were described in recent years using quantitative analysis methods [12–18]. Typically, in larvae, taxis involves regulating two stereotyped motor patterns: runs, which are periods of forward crawling and turns which are reorientation events involving head sweeps (one or multiple) followed by a choice of direction [12, 13, 16, 19, 20]. It is thought that larvae compare sensory information over time during a run and turn when they detect a change in sensory input for the worse (e.g. a decrease in the concentration of an attractive odor, or an increase in aversive light intensity) [12, 13, 16]. Thus, larvae are more likely to turn when they are crawling in the unfavorable direction (away from attractive or towards aversive cues), than in the favorable direction (towards attractive or away from aversive cues). Comparison of sensory information during an exploratory head sweep is thought to determine the direction of the turn [12, 13, 16, 20]. Thus, larvae are more likely to accept head sweeps (and turn in that direction) during which there is a change for the better, than those during which there is a change for the worse. Larvae have also been shown to modulate the size of turns and make bigger turns towards favorable conditions than towards unfavorable conditions. Larvae use these same strategies when navigating gradients of odors (chemotaxis), CO_2, light (phototaxis) and temperature (thermotaxis) [12–14, 16, 19]. Bigger third instar larvae, but not smaller second instar larvae also appear to perform a spatial comparison of olfactory input on the left and right side of their body during chemotaxis, as they are more likely to perform the first head sweep after a run towards the favorable direction [16].

The sensory neurons and receptors that mediate taxis in some types of sensory modalities (odor, temperature, light, CO_2) in *Drosophila* larvae have also been extensively investigated [13–15, 17, 20–23]. Some central neuron types have also been identified [24]. For examples the lateral neurons (LNs) downstream of photoreceptor neurons and a pair of neurons in the brain have been shown to be implicated in phototaxis [12, 25, 26], a central neuron pathway have been identified for odor-tracking [27] and the SEZ as a premotor center has been shown to regulate the selection of behavioral programs based on the integration of sensory stimuli of different modalities [28]. However, despite these findings, the central components of the neural circuits underlying taxis strategies (regulating when to turn, which way to turn, and how much to turn) are still poorly understood.

Adult flies orient in response to air-currents during flight and in the context of response to odor plumes [5, 7, 29]. It is unknown whether *Drosophila* larvae can perform anemotaxis, and if so, if they do so via the strategies used during chemotaxis, phototaxis, and thermotaxis.

Here we used a high-throughput behavioral assay combined with quantitative behavioral analysis to show *Drosophila* larvae perform negative anemotaxis. We found they use similar strategies as during chemotaxis, phototaxis, and thermotaxis: they modulate turn probability, direction and size to move away from high wind speeds and away from the direction of the wind. We then combined the high-throughput quantitative behavioral analysis methods with manipulation of neuronal activity (silencing using tetanus toxin) and determined two types of mechanosensory neurons that together contribute to anemotaxis: chordotonal and multidendritic class III neurons. In a targeted behavioral inactivation screen, we found seven candidate central neuron types involved in anemotaxis. By reconstructing the neurons in an EM volume of the larval nervous system we identified local interneurons, and first- and second-order SEZ and brain projection neurons of the anemotaxic circuit. We also found that silencing a dopaminergic brain neuron type impaired anemotaxis. Altogether, these neurons represent the starting points for determining the circuit mechanisms that implement sensorimotor decisions during anemotaxis.

Results

Drosophila larvae perform negative anemotaxis

To determine whether *Drosophila* larvae can anemotax, we presented fixed spatial gradients of wind speed to large numbers of animals while tracking their motion to analyze their behavioral dynamics.

We generated gradients of air-current speeds with one end of the arena at high wind speeds and the other at low wind speeds. We tested two different gradients: one gradient was between 3 m/s and 1 m/s and a second between 5 m/s and 2 m/s. The gradient of wind speeds is generated along the x axis in the arena. At the start of the assay we placed larvae in the center of each agar plate in a line along the y axis, perpendicular to the gradient of wind speeds, and monitored their behavior for 10 min. We found that at the end of the experiment the majority of the larvae were located at or near the lower speed end (Figure 1A). To quantify the overall taxis performance of *Drosophila* larvae in an air-speed gradient we computed the navigational index by dividing the mean velocity of all larvae in the x direction, $\langle v_x \rangle$, parallel to the wind gradient, by the mean crawling speed, $\langle s \rangle$

$$Nind_x = \langle v_x \rangle / \langle s \rangle$$

A navigational index of +1 would correspond to all larvae moving straight down the gradient, a navigational index of −1 to all the larvae moving straight up the gradient and a navigational index of 0 to larvae moving without bias towards 0° or 180° (down or up the gradient).

The navigational index in the x-axis was 0.17 in a 3 to 1 m/s gradient and 0.37 in a 5 to 2 m/s gradient. In contrast, navigation index in the y-axis (along which there was no gradient of wind-speed) was close to 0 (Figure 1B). In a control experiment with no air-current, the navigation index was close to 0 as expected (Figure 1B, Data S1). Thus, larvae anemotax away from the direction of the wind and towards lower air speeds in both the 3 to 1 m/s and 5 to 2 m/s air current gradients.

Behavioral strategies in anemotaxis

In order to uncover the behavioral strategies that larvae use during anemotaxis, we monitored the actions of individual larvae (running, head sweeping, or turning) of 830 intact attP2>TNT larvae during anemotaxis, using a previously published quantitative behavioral analysis method [12–14]. We then computed population statistics for features that reveal how larvae bias their trajectories towards the areas of the arena with slower wind speeds and away from the direction of the wind. Because larvae anemotax more efficiently in stronger wind speeds we chose the 5 to 2 m/s gradient for the more detailed analysis (Figure 1A–D).

As for other types of taxis behaviors [12–14, 16, 19, 20], larvae alternate runs (periods of forward crawling in approximately straight trajectories) with turns which allow them to change the direction of heading (Figure 1A, 1C, and 1D). We analyzed whether and how runs and turns were modulated as a function of four different headings in the wind-speed gradient: down the gradient, up the gradient, and the two headings perpendicular to the gradient (Figure 2A–H, Figure S1A–H).

We found larvae have a lower probability of orientation towards the wind (upwind) than away from the wind (downwind) (measured as a fraction of time larvae spend crawling down and up wind-speed gradients, respectively), i.e. there is a higher probability that larvae will be found oriented down the wind-speed gradient, than up the gradient (Figure 2A, Data S3). Larvae also crawled slightly slower when heading up air-speed gradients than down (Figure 2B).

To test whether larvae reorient themselves with respect to the wind-speed gradient during runs, we computed the mean heading change during runs as a function of larval heading at the start of the run. The mean heading change was nearly zero regardless of the initial heading so the larvae did not reorient themselves during runs in wind-speed gradients (Figure 2C).

Reorientation thus mostly occurs during turns. We examined the rate at which larvae turned as a function of heading. The turn rate was highest when the larvae were heading up the wind-speed gradient and lowest when heading down the gradient (Figure 2D). Thus, as described for other types of taxis [12, 13, 16, 17, 19], larvae decreased their turn rate when headed in a favorable direction and increased their turn rate when headed in an unfavorable direction.

We also examined whether larvae modulate the size of turns, as a function of heading prior to the turn (Figure 2E). We found that larvae tend to make larger turns (average 94° change

in direction) when previously headed up the wind-speed gradient (towards 180°) and smaller turns (average 65°) when headed downwind (0°).

We also found larvae bias the direction of turns when crawling along the axis perpendicular to the wind-speed gradient (Figure 2F). We found that nearly 67% of turns were downwind, and only 33% of turns were towards the upwind (Figure 2F).

Furthermore, we found that the direction of the first head sweep after a run was already biased towards the lower wind-speed side (Figure 2G).

In addition, we observed a significantly higher probability of accepting a head sweep when facing the lower wind-speed side, relative to the higher wind-speed side ($p<0.0001$) (Figure 2H).

In summary, larvae mostly use similar strategies during anemotaxis as those previously described for other types of taxes: they modulate the rate, size, and direction of turns [12, 13, 16, 17]. They even modulate the direction of the first head sweep towards the favorable side, as has been reported for third instar larvae during chemotaxis [16]. However they do not modulate the orientation of runs during crawling as has been observed in chemotaxis [30].

Chordotonal and multidendritic class III sensory neurons are involved in anemotaxis

We have previously identified the chordotonal (cho) sensory neurons on the body wall of the larvae that mediate on-off responses to air-current [31–33] in a behavioral assay with uniform speeds in the arena. Here, we asked whether these sensory neurons also mediate anemotaxis of *Drosophila* larvae (Figure 3A–C, and Figure S2A–C). We found that when we silence the cho neurons using tetanus toxin (TNT) [34] (*cho>TNT*) in a 5 to 2 m/s wind-speed gradient, larvae perform anemotaxis less efficiently: their navigational index was significantly reduced compared to control larvae (Figure 3A, Data S1) and they show a lower probability of orientation away from the wind compared to the control (Figure S2C, Data S3). The navigational index normalizes for run speed, so changes in baseline locomotion speed should not cause changes in the navigation index. We nevertheless wondered whether larvae with silenced cho neurons exhibit locomotion defects [35] in addition to anemotaxis defects (Figure S2B). We found that silencing cho neurons did not significantly reduce the mean speed during runs in the absence of stimuli under our experimental conditions, in fact these larvae showed slightly increased mean speed during runs (Figure S2B).

Although larvae with silenced cho neurons are not efficient in anemotaxis (i.e. they have a significantly lower navigation index compared to controls), when we examined individual behavioral strategies, we found that they were not significantly reduced compared to controls (Figures 3B–C, Data S3–S4). The poor navigational performance could be due to a cumulative effect of slight non-significant perturbations of individual behavioral strategies.

Since silencing of cho sensory neurons only moderately impaired anemotaxis, this suggests that other types of sensory neurons may also be involved in sensing the wind speed. We therefore tested another type of sensory neurons that was shown to mediate light touch and on-off responses to air current [36, 37]: the multidendritic class III neurons (md III) [33]

(Figure 3A–C, Figure S2A–C, and Data S1). Silencing of md III neurons resulted in slightly lower but not significantly different navigational performance compared to the *attP2>TNT* control (Figure 3A, Data S1). We further analyzed the behavioral strategy in *md III>TNT* larvae and found no strategy that was significantly different from the control (Figure 3 B–C, Data S3–S4).

Different sensory modalities can act together by providing independent estimates of the same event that can be combined to improve sensitivity and reduce ambiguity [38–41]. Cho neurons sense vibration and the deformation of the cuticle as a result of mechanical pressure [31, 42]. The md III neurons sense the light touch through ion channel activated by small forces [37, 43]. Combining sensory information from these two independent modalities could result in improved sensing of wind speeds [40]. We therefore silenced both cho and md III neurons to test whether there was a greater effect from silencing the two modalities together, compared to either one alone. These larvae had a significantly lower navigational index compared to the controls, and compared to *md III>TNT* larvae (Figure 3A, Data S1). Their navigation index was also lower than of *cho>TNT* larvae, although the effect did not reach significance. However, we found that while silencing either modality alone did not significantly impair individual strategies, silencing both modalities did significantly impair some of the strategies compared to controls (Figure 3B–C). Thus, the probability of turning downwind from a perpendicular direction was significantly lower compared to control larvae (Figure 3B). The difference in acceptance rates of head sweeps away and toward the wind was also significantly reduced compared to control larvae, as well as compared to larvae in which we silenced individual modalities (Figure 3C).

Silencing of both cho and md III neurons simultaneously resulted in a more severe phenotype in anemotaxis than silencing of individual sensory types. This suggests cho and md III neurons may synergistically contribute to anemotaxis.

Because silencing of both cho and md III neurons simultaneously affected the choice of turn direction, rather than turn probability and turn size, these sensory types may have a key role in comparing the sensory information during exploratory head sweeps and the choice of turn direction.

Identifying central neurons whose silencing leads to reduced performance in anemotaxis

In order to identify neurons in the central nervous system involved in anemotaxis, we performed a targeted screen of 205 sparse GAL4 and intersectional Split GAL4 lines (Figure S3A–C, Figure 4A, Figure S4A–B, Table S1). These 205 lines were selected in an anatomical prescreen for lines that drive expression in single or in few neuron types. Because generally larvae are more efficient in anemotaxis in stronger wind-speed gradients (Figure 1B, Data S1), we chose the 5 to 2 m/s gradient for the screen. The silencing was performed with TNT as using temperature inducible effectors is technically challenging in air-puff experiments. The air at high speeds would cool down the set up and it is difficult to maintain stable high temperatures (ca. 35°C) of the larvae and the arena for the duration of the experiments.

We identified eight neuronal lines in which the silencing of neurons resulted in less effective taxis (their navigational index was significantly lower compared to controls) (Figure 4A). As a control, we also quantified the navigational index in y axis for each of the lines to confirm that the navigation index (in x axis) is indeed due to the gradient of wind speeds. We found that for all of the lines, the navigational index in y axis during anemotaxis was around 0 as expected (Figure S4B, Data S1).

We further examined which type of behavioral strategy caused the poor navigational performances observed in each line.

We first analyzed the modulation of the turn rate, specifically whether these lines fail to decrease their turn rate when heading in the favorable direction and fail to increase their turn rate when facing unfavorable directions (Figure 2D). We found that in all of the eight lines the turn rate was comparable to controls (Data S3).

Similarly, all lines retained the ability to modulate the size of turns as a function of sensory gradient (Data S3).

Finally, we examined how the choices of turn direction were affected in the lines with poor navigational performances (Figures 4B–C).

We found that silencing of neurons in line *SS01632* resulted in a significantly decreased probability of turning downwind from a perpendicular direction compared to controls (Figure 4B, Data S4). Interestingly, this strategy is also affected when silencing both cho and md III neurons (Figure 3, Data S4).

Silencing of neurons in the *SS01401* line resulted in a loss of bias for performing the first head sweep away from the direction of the wind (Figure 4C, Data S4). Silencing of neurons in the *SS01948* line even appears to reverse the bias of first head sweep toward the direction of the wind (Figure 4C, Data S4).

Thus, amongst the eight lines with less efficient anemotaxis there were three lines with defects in two different types of strategies: in the choice of turn direction or first head sweep direction during anemotaxis.

In order to investigate whether some of the neurons that contribute to anemotaxis also contribute to baseline locomotion, we recorded the locomotion without any stimulation in larvae expressing TNT in each of the positive hit driver lines. We computed the mean speed in runs in silencing and control experiments. We next computed the 95% confidence interval on the ratio of the inactivated lines mean run speed to the control mean run speed (Figure S4A, Data S2). For most of the CNS neuron lines the confidence interval includes 1, so we cannot say that the speeds are not the same.

Three of the CNS lines have mean speeds that are significantly lower than the controls (*SS00721, SS00878, SS01948*). The navigational index normalizes for run speed, so changes in run speed cannot directly cause changes in the navigation index reported in Figure 4. *SS01948>TNT* larvae also have a defect in biasing the direction of the first head sweep: they bias the first head sweep upwind instead of downwind, i.e. they make the

opposite choice to controls (Figure 4C). This defect cannot be explained in terms of a general locomotor defect, nor an effect on mean speed. Thus, some of the neurons identified in our screen may have multiple roles in behavior, both during anemotaxis and in controlling baseline crawling speed.

Electron microscopy reconstruction of identified neurons reveals portions of the larval anemotaxis circuit

In order to better understand the circuits underlying anemotaxis, we wanted to identify the neurons that were targeted by the eight central nervous system (CNS) lines and either identify or reconstruct them in a an electron microscopy (EM) volume of the larval nervous system to reveal their connectivity [32, 38, 44].

We first characterized the morphology of the neurons in each line using light-microscopy, by labelling them with GFP, or when necessary using multicolor flip-out (MCFO) [45] (Figure 5A–H and Figure S5A–D). We found that six lines drove expression in nerve cord neurons (Figure 5A–F), one in central brain neurons (Figure 5G), and one in two neurons in the subesophageal zone (SEZ) and one in the posterior end of the nerve cord (Figure 5H). Five of the nerve cord lines drive expression in just a single neuron type. The *SS00721* drives expression strongly in a pair of thoracic neurons, that project to the brain (that we named Recliner), and weakly in an abdominal neuron pair, which is therefore unlikely to contribute to the behavioral phenotype obtained with that line.

To determine the identity of the neurons, we compared the light microscopy images of these neurons to a database of all previously known larval neurons that were reconstructed with EM [32, 38]. However, if a neuron was unknown and not yet reconstructed with EM, we would not find it in this database. Previously, only the local partners of cho sensory neurons in the A1 abdominal segment were reconstructed [32, 38], but not the long-range partners. Some, but not all partners of md III sensory neurons had also been reconstructed.

We found that three lines drove expression in previously reconstructed nerve cord neurons with known connectivity, but unknown function. Two of these neurons receive direct synaptic input from md III neurons: a projection neuron that ascends to the SEZ, A09e [46] (*SS00878*), and a local abdominal neuron chair-1 (A10a) (*SS00911*) [38] (Figure 5A–B, Figure 6 and Figure S5D). Another local inhibitory interneuron, drunken-4 (*SS01401*) receives direct synaptic input from cho neurons [32] (Figure 5C, Figure 6, and Figure S5B).

Three lines, *SS00721*, *SS00886*, and *SS01632*, drove expression in unknown nerve cord neurons that have previously not been reconstructed in the EM volume. Using cell bodies and primary backbone positions as a guide, we identified several candidate neurons for each line and traced each candidate until they could be excluded based on morphology. After several iterative rounds, one candidate emerged for each line. These neurons were then reconstructed to completion, including all arbors and pre- and postsynaptic connections. This work revealed three novel long-range projection neurons either directly, or indirectly downstream of cho sensory neurons: Jupiter, which collects inputs from the VNC and ascends to the SEZ (Figure 5D, Figure 6, and Figure S5D); Recliner, which primarily receives thoracic inputs and ascends to the brain (Figure 5E, Figure 6 and Figure S5C); and

Thoracic ladder-1, which spans many thoracic and abdominal segments (Figure 5F and Figure 6). Jupiter and Thoracic ladder-1 receive direct cho inputs while Recliner receives inputs from the first order cho partners: Jupiter (Figure 6, Data S5). Thus, Drunken-4, Jupiter, and Recliner make a pathway from the mechanosensory cho neurons to the brain (Figure 6).

EM correlates of *SS00854* were not identified. This line drives expression equally strongly in two types of SEZ neurons and a pair of abdominal neurons, so it is not possible to speculate whether the phenotype is due to abdominal or SEZ neurons.

The central brain line (*SS01948*) was matched with the pPAM cluster of dopaminergic neurons (DANs), that innervate the medial lobe of the mushroom body [47, 48] (Figure 5G and6), surprisingly suggesting that these mushroom body DANs are involved in anemotaxis.

Discussion

Using targeted genetic manipulation of neuronal activity combined with quantitative analysis of locomotor behaviors and EM reconstruction of synaptic connectivity, we characterize for the first time the behavioral dynamics and the candidate neural substrates underlying anemotaxis in *Drosophila* larvae.

We determined that larvae move down the gradient, away from strong air-currents (winds), and identified the behavioral strategies that larvae use to achieve this behavior. Overall, we found that larvae use similar strategies during anemotaxis as during taxis in other types of sensory gradients: they modulate the probability, size and direction of turns as a result of sensory input. They chose the direction of turn by performing one or more head-sweeps during each reorientation event. Larvae are more likely to reject head sweeps in the direction of higher wind speeds and accept head sweeps in the direction of lower wind speeds (i.e. they are more likely to turn in the direction of lower wind speeds). This is consistent with the idea that larvae perform temporal comparisons of sensory information during left and right head sweeps, as proposed for other taxes behaviors. Interestingly, we found that during anemotaxis larvae also bias the direction of the very first head sweep after a run towards the favorable direction. This suggests that during anemotaxis larvae are also able to use the somatosensory system to perform a spatial comparison of sensory information on the left and right side of the body to bias the direction of the first head sweep. Previous studies showed that the first head sweep was unbiased in odor and CO_2 gradients in second instar larvae, but it was biased in odor gradients in third instar larvae [13].

We found that silencing cho sensory neurons impaired anemotaxis, however, it did not abolish it, and it did not have a significant effect on individual strategies. Silencing md III neurons alone did not result in a significant impairment in anemotaxis. However, silencing of both cho and md III neurons simultaneously resulted in a severe phenotype and a significant defect in the choices of turn direction. This suggests that these two sensory modalities together mediate temporal comparisons during exploratory head sweeps to modulate the direction of turns.

It should be noted that silencing cho and md III neurons did not completely abolish anemotaxis, suggesting that additional sensory neurons might be involved. External sensory neurons on the body wall are potential candidates to mediate wind related behaviors, based on their morphology [49, 50].

In a behavioral inactivation screen, we identified eight lines with impaired anemotaxis. Silencing some of these neurons (Thoracic ladder-1, pPAM DANs, drunken-4) significantly affected either the choice of turn direction, or the choice of first head sweep. Thus, different types of strategies could be controlled independently. It is also possible that some strategies are redundantly regulated by multiple neuron types, so silencing one type alone does not produce a significant defect. Modulation of turn and first head sweep direction could be more susceptible to perturbation of activity in single circuit elements.

Based on EM reconstruction we determined six of the neurons involved in anemotaxis were directly or indirectly downstream of cho or md III neurons. Three nerve cord neurons received direct sensory input from cho neurons. A fourth neuron is a second order cho partner, receiving input from the first order partner, Jupiter. The two other VNC neurons receive input from md III neurons. Interestingly, three of the VNC neurons are ascending projection neurons. A09e and Jupiter receive input from md III and cho neurons, respectively, and then both project to the subesophageal zone (SEZ). It was previously shown that a group of neurons in the SEZ modulates the probability of transitioning between runs and turns based on information from multiple sensory modalities [28]. The SEZ could thus be the hub where sensory information for multiple modalities converge, including cho and md III pathways, to modulate sensorimotor decisions during orientation behaviors. In addition to the SEZ, our study suggests brain contributes to anemotaxis, as we identified an ascending neuron that projects to the brain and PAM-cluster DANs in the brain whose silencing using the *SS01948* line surprisingly impairs anemotaxis.

In natural environments, taxis is rarely performed in the presence of stimuli from a single modality. Rather, larvae combine sensory information from multiple modalities and often navigate across conflicting sensory gradients. For this reason, some of the circuitry that underlies taxis strategies could be shared between different types of taxes. The idea of an overlapping circuitry for taxes in different types of sensory gradients is further supported by the findings that all described taxes so far (including anemotaxis) comprise similar strategies. Identifying circuit elements of anemotaxis in higher order centers, i.e. the SEZ and brain, can therefore help elucidate universal circuit mechanisms of sensorimotor decision-making in sensory gradients. For example, our findings suggest that PAM-cluster DANs are implicated in taxis. These neurons synapse onto the medial lobe of the mushroom body, an integrative structure of the insect brain and therefore could be involved in decision-making in other modalities, not only during anemotaxis [48, 51]. We also found that inactivating these DANs resulted in significantly decreased mean speed during runs. In the adult *Drosophila*, DANs show context and state movement related responses [52, 53] while midbrain DANs in vertebrates were shown to be involved in movement initiation, movement vigor, decision-making and learning [54–57]. Thus, these *Drosophila* DANs could be modulating the activity of higher-order centers in the mushroom body depending on the multisensory context or animal's behavioral states [57, 58]. It will important to further

investigate the implication of the DAN neurons in anemotaxis and other types of taxes by using different drivers and other type of effectors for neuronal manipulation (i.e. temperature inducible) where possible.

Studying the neural basis of taxis in the genetically tractable *Drosophila* larva has many advantages. Neuronal activity can be manipulated, the connections between neurons determined by EM reconstruction [32, 38, 44, 48, 59–63], and patterns of neuronal activity can be correlated with behaviors. The novel candidate elements of the anemotactic circuitry identified in this study provide an excellent starting point for further studies using other types of neuronal manipulations and physiology to investigate the role of each individual neuron. In addition, they provide an entry point into the neuronal pathways and circuit mechanisms underlying taxis from the sensory inputs to higher, more integrative regions of the brain by using a combination of approaches available in the *Drosophila* larvae: quantitative behavioral analysis, optogenetics and the monitoring of neuronal activity in a behaving animal [64].

STAR Methods

CONTACT FOR REAGENTS AND RESOURCE SHARING

Further information and requests for resources and reagents should be directed to and will be fulfilled by the Lead Contact, Tihana Jovanic (jovanict@janelia.hhmi.org)

EXPERIMENTAL MODEL AND SUBJECT DETAILS

Drosophila Stocks—We used GAL4 from the Rubin collection available from Bloomington stock center each of which is associated with an image of the neuronal expression pattern shown at http://flweb.janelia.org/cgi-bin/flew.cgi. We used GAL4 lines (*R61D08* for chordotonals, *19–12-GAL4* for multidendritic class III [44]) in behavioral experiments and generate intersectional lines (Split lines: *SS00721*, *SS00854*, *SS00878*, *SS00886*, *SS00911*, *SS01401*, *SS01632*, *SS01948*). In addition we used the insertion site stocks, w;;attP2 and w;attP2;attP40 [65, 66], as well as w;iav-GAL4;UAS-TNT-e stock. We used the progeny larvae from the insertion site stocks, w;;attp2, and w;attP2;attP40 crossed to the appropriate effector (UAS-TNT-e (II)) for characterizing larval behavior during anemotaxis. w;; attP2 and w;attP2;attP40 were selected because they have the same genetic background as the GAL4 and Split-GAL4 tested in the screen. We used the following effector stocks: UAS-TNT-e [34] and pJFRC12–10XUAS-IVSmyr::GFP (Bloomington stock number: 32197). We also used Canton S (the background of the UAS-TNT-e stock) to cross GAL4 and Split-GAL4 drivers with in GAL4 controls.

METHOD DETAILS

Larva dissection and immunocytochemistry—To analyze the expression pattern of the GAL4 and SplitGAl4 lines, we crossed the lines to pJFRC12–10XUAS-IVSmyr::GFP (Bloomington stock number: 32197; [23]). The progeny larvae were placed in a phosphate buffered saline (PBS; pH 7.4) and fixed with 4.0% paraformaldehyde for 1–2 hr at room temperature, and then rinsed several times in PBS with 1% Triton X-100 (PBS-TX). Tissues when then mounted on poly-L-lysine (Sigma-Aldrich) coated coverslips and then transferred

to a coverslip staining jar (Electron Microscopy Sciences) with blocking solution, 3% normal donkey serum in PBS-TX for 1 hr. Primary antibodies were used at a concentration of 1:1000 for rabbit anti-GFP (Invitrogen) and 1:50 for mouse antineuroglian (Developmental Studies Hybridoma Bank) and 1:50 for anti-N-cadherin (Developmental Studies Hybridoma Bank) and incubated for 2 days at 4°C. Tissues when rinsed multiple times in PBS-TX and then incubated for 2 days. with secondary antibodies: anti-mouse IgG Alexa Fluor 568 Donkey (diluted 1:500; Invitrogen), Alexa Fluor 647 Donkey anti-rat IgG (1:500, Jackson ImmunoResearch) and fluorescein FITC conjugated Donkey anti-rabbit (diluted 1:500; Jackson ImmunoResearch). After incubation, the tissue was rinsed for several hours in PBS-TX, and dehydrated through a graded ethanol series, cleared in xylene and mounted in DPX (Sigma). Images were obtained with 40x oil immersion objective (NA 1.3) on a Zeiss 510 Confocal microscope. Images of each nervous system were assembled from a 2x array of tiled stacks, with each stack scanned as an 8-bit image with a resolution of 512×512 and a Z-step of 2 μm. Images were processed using Fiji (http://fiji.sc/) and ImageJ (https://imagej.nih.gov/ij/).

Behavioral apparatus—The apparatus was described previously [31, 32]. Briefly, the apparatus comprises a video camera (DALSA Falcon 4M30 camera) for monitoring larvae, a ring light illuminator (Cree C503B-RCS-CW0Z0AA1 at 624 nm in the red), a computer (see [31] for details; available upon request are the bill of materials, schematic diagrams and PCB CAM files for the assembly of the apparatus) and a hardware modules for controlling air-puff, controlled through multi worm tracker (MWT) software (http://sourceforge.net/projects/mwt) [67], as described in [31]. Air-puff is delivered as described previously [31]. Briefly it is applied to a 25625 cm2 arena at a pressure of 1.1 MPa through a 3D-printed flare nozzle placed above the arena (with a 16 cm 6 0.17 cm opening) connected through a tubing system to plant supplied compressed air (0.5 MPa converted to a maximum of 1.4 MPa using a Maxpro Technologies DLA 5–1 air amplifier, standard quality for medical air with dew point of 210°C at 90 psig; relative humidity at 25°C and 32°C, ca. 1.2% and 0.9%, respectively). The strength of the airflow is controlled through a regulator downstream from the air amplifier and turned on and off with a solenoid valve (Parker Skinner 71215SN2GN00). The gradient is achieved by adjusting the inclination of the nozzle delivering the air-current to the arena. The gradient of air-flow speeds is parallel to the direction of air-flow and decreases with the distance from the nozzle (source of wind). The nozzle is fixed with a system of screws to prevent any movement during and in between experiments. Air-flow rates were measured before each round of experiments at 9 different equidistant positions in the arena with a hot-wire anemometer to ensure that the speed was 5 m/s at one end and on the opposite end 2 m/s for the 5–2 m/s gradient and 3 m/s and 1 m/s respectively, for the 3–1 m/s gradient (Extech Model 407119A and Accusense model UAS1000 by DegreeC). The air-current relay is triggered through TTL pulses delivered by a Measurement Computing PCI-CTR05 5-channel, counter/timer board at the direction of the MWT. The onset and durations of the stimulus is also controlled through the MWT.

Behavioral Experiments—Embryos were collected for 8–16 hours at 25°C with 65% humidity. Larvae were raised at 25°C with normal cornmeal food. Foraging third instar larvae were used (larvae reared 72–84 hours or for 3 days at 25°C).

Before experiments, larvae were separated from food using 10% sucrose, scooped with a paint brush into a sieve and washed with water (as described previously). This is because sucrose is denser than water, and larvae quickly float up in sucrose making scooping them out from food a lot faster and easier. This method is especially useful for experiments with large number of animals. We have controlled for the effect and have seen no difference in the behavior between larvae scooped with sucrose and larvae scooped directly from the food plate with a pair of forceps.

The larvae were dried and spread on the agar in a line in the center of the arena along the y-axis perpendicular to the gradient of air speeds. The substrate for behavioral experiments was a 3% Bacto agar gel in a 25625 cm2 square plastic dishes. Larvae were washed with water at room temperature, the dishes were kept at room temperature and the temperature on the rig inside the enclosure was set to 25°C.

The humidity in the room is monitored and held at 58%, with humidifiers (Humidifirst Mist Pac-5 Ultrasonic Humidifier).

We tested approximately 20–30 larvae at once in the behavioral assays. For each genotype, we did at least 3 repetitions (see Table S2 for N of animals and experiments for each genotype). The temperature of the entire rig was kept at 25 °C. In the assay, the larvae were put in the center of the plate in a line perpendicular to the gradient axis immediately prior the stimulus delivery. The air-puff was delivered continuously from the beginning of the experiment (time 2s after start of recording) and then for 10 minutes. We have used 3 m/s −1 m/s and 5 m/s to 2 m/s wind-speed gradients. The 3 m/s to 5 m/s wind speeds corresponds to what is on wind scale is referred to as a strong breeze. At this wind speed the small branches on trees start to be moved by the wind. We have found that between 3 m/s - 8 m/s larvae respond strongly, but the response starts saturating around 6 m/s. The navigational performance was better in the higher gradient (5 m/s-2 m/s compared to the 3 m/s-1m/s gradient) as shown in Figure 1D. That was the reason we chose this gradient for further studies. All the data from Figure 2 and on are obtained in a higher 5 m/s-2 m/s gradient.

Electron Microscopy Reconstruction and Wiring Diagrams—EM reconstruction was performed using a complete CNS serial section transmission EM volume from a 6-hour old *Canton S G1* × w^{1118} *[5905]* larva, with a resolution of 3.8nm x 3.8nm x 50nm [38]. Reconstruction and synapse annotation followed previous protocols [44, 48] using the web-based annotation software, CATMAID [68]. To identify neurons of interest covered by our split-GAL4 lines, we performed exploratory tracing downstream of mechanosensory chordotonals in segment A1. Gross morphologies, including axon bouton, dendrite, and cell body positions, were compared to light microscopy images to positively identify neurons in EM. Identified neurons were then fully reconstructed, including all synapses and fine dendritic processes. If hemilateral pairs of neurons received at least 3 synapses from a particular mechanosensory chordotonal type on both sides, we considered them strong downstream chordotonal partners.

QUANTIFICATION AND STATISTICAL ANALYSIS

Behavioral analysis—Larvae were tracked in real-time using the MWT software [67]. We rejected objects that were tracked for less than 5 seconds or moved less than one body length of the larva. For each larva MWT returns a contour, spine and center of mass as a function of time. From the MWT tracking data we computed the key parameters of larval motion, using the MAGAT analyzer software package (https://github.com/samuellab/MAGATAnalyzer) that we adapted to the MWT format [13]. Further analysis was carried out using custom MATLAB scripts described previously [13] software to identify behaviors, especially runs, turns, and head sweeps.

To calculate statistics involving center-of-mass movement along larval trajectories (for example, distributions of instantaneous heading and speed in Figures 2 and Figure S1 and navigational indices in Figures 1, 3 and 4) we needed to estimate the number of independent observations of quantities of center-of-mass movement along each larval trajectory. To do this, we calculated the autocorrelation function of the direction of motion,

$$C(\tau) = \langle \hat{v}(t) \cdot \hat{v}(t+\tau) \rangle_t$$

and extracted the time constant, T, of its component of exponential decay,

$$C(\tau) = e^{-\tau/\mathrm{T}}$$

This correlation time constant was typically ~20 s. To calculate the s.e.m. of center-of-mass motion statistics, we estimated the number of independent observations as the total observation time for each measurement divided by twice the correlation time constant. For more details see [13].

Screen design—We screened a total of 205 Drosophila lines: 37 GAL4 lines from the Rubin GAL4 collection [65, 69] and 168 Split-GAL4 lines made based on the GAL4 lines in the Rubin collection. We silenced small subsets of neurons and individual neurons in these lines using tetanus toxin. We selected these lines from the entire collection for sparse expression in the brain and ventral nerve cord of the larval CNS as well as expression in the sensory neurons The intersectional Split-GAL4 lines were designed based on the overlapping expression patterns of GAL4 driver lines. In addition for sparseness, some lines were chosen to be screened based on results from a previous air-puff inactivation screen (without gradient) [33] (images of the larval CNS are available at http://www.janelia.org/gal4-gen1).

The N of detected navigational events (N of runs, reorientations) is given in Table S2.

Hit detection and statistical analysis—The hits were determined based on the overall navigational performance of each GAL4 and Split-GAL4 lines. Hits were considered the lines that were significantly different compared to their respective controls: w;;attP2 for GAL4 lines and w;attP2;attP40 for Split-GAL4 lines. We focused the study on eight of the

strongest hits (some lines were excluded of the study as they had showed stochastic neuronal expression patterns).

Error bars and p-values were generated using a bootstrapping procedure.—A set of experiments consisted of repeated presentations of the same stimulus to different groups of animals of the same genotype. For each set of experiments, we reported the mean measurement (e.g. of navigational index) across all the animals in all experiments. We sought to determine how much we might expect that mean measurement to vary if we repeated the entire set of experiments over and over again.

The standard way to estimate the variation of the mean is to calculate the standard error of the mean, dividing the standard deviation of all measurements by the square root of the number of measurements. This method is appropriate if all animals and events are assumed to be drawn from the same random distribution. However, if there are correlated sources of noise, e.g. under-expression of genes in a subset of the larvae tested, this method can underreport the expected variance in the mean.

We therefore adopted a bootstrapping approach that preserved potentially correlated sources of noise, and we calculated p-values without assuming Gaussian statistics off the data set. To generate a single bootstrap for a set of experiments, we

1. Selected an experiment, E_i at random from the set of N experiments.
2. Selected a random subset, with replacement, of T_i tracks from that experiment, where T_i is the total number of tracks in the selected experiment.
3. Repeated 1–2 until we had sampled T_{total} of tracks, where T_{total} is the total number of tracks in the original data set.
4. We then analyzed the set of tracks as though it were a new experiment and found the mean navigational index, probability of turning away from the wind, etc.

We repeated the bootstrapping procedure (steps 1–4) 3000 times and then analyzed the bootstrap results as follows:

The standard error of the mean (error bars in figures) was calculated as the standard deviation of the set of bootstrapped means.

The p-value of a comparison is the fraction of the 9,000,000 (3,000 × 3,000) bootstrap pairs in which the opposite effect was observed. For instance, if the navigational index of an inactivated line was lower than the control navigational index, the p-value is the probability a navigational index randomly chosen from the bootstrapped inactivated set would be higher than a navigational index randomly chosen from the bootstrapped control set. This non-parametric method does not require assumptions about the normality of the data [70].

For the controls in Figure 1 and 2 with large sample sizes (N of experiments > 50) the comparisons between no wind gradient and wind gradient conditions and 3 m/s to 1 m/s and 5 m/s and 2 m/s gradient (Figure 1) and probabilities of turning and headsweep decisions

towards and away the direction of the wind (upwind and downwind) (Figure 2F–H, Figure SF–H) were done using an unpaired t-test.

For no stimulus conditions, we calculated, with 95% confidence, a confidence range for the ratio of mean speeds in inactivation experiments to the control experiments.

DATA AND SOFTWARE AVAILABILITY

All data are included in Tables S1–S2 and Data S1–S5 or are available from the authors upon request

The Multi Worm tracker software is available at: https://sourceforge.net/projects/mwt/

The MAGAT software package is available at: https://github.com/samuellab/MAGATAnalyzer

Supplementary Material

Refer to Web version on PubMed Central for supplementary material.

Acknowledgments

We thank Yuh Nung Jan (UCSF) and Javier Valdes Aleman for fly stocks. We thank Fly core (especially Monti Mercer and Brandi Sharp) at JRC for fly crosses, Rebecca Arruda and Tam Dang for help with the behavioral experiments, Casey Schneider-Mizell for helpful discussions regarding neuronal connectivity, Nadine Randel for naming a neuron, Benjamin Cocanougher for the larva drawing in the Graphical abstract, Rex Kerr for assistance with MWT. We thank the Janelia Visitor Project for Marc Gershow's visits.

Reference

1. Casas J, and Steinmann T (2014). Predator-induced flow disturbances alert prey, from the onset of an attack. Proc. Biol. Sci 281, 20141083–20141083. [PubMed: 25030986]
2. Togunov RR, Derocher AE, and Lunn NJ (2017). Windscapes and olfactory foraging in a large carnivore. Sci. Rep 7, 46332. [PubMed: 28402340]
3. Van Tilborg M, Sabelis MW, and Roessingh P (2004). State-dependent and odour-mediated anemotactic responses of the predatory mite Phytoseiulus persimilis in a wind tunnel. Exp. Appl. Acarol 32, 263–270. [PubMed: 15176731]
4. Yu YSW, Graff MM, Bresee CS, Man YB, and Hartmann MJZ (2016). Whiskers aid anemotaxis in rats. Sci Adv 2, e1600716–e1600716. [PubMed: 27574705]
5. Kalmus H (1942). Anemotaxis in Drosophila. Nature 150, 405–1.
6. Schooley RL, and Branch LC (2005). Limited perceptual range and anemotaxis in marsh rice rats Oryzomys palustris. Acta Theriologica, 59–66.
7. Spencer Johnston J (1981). Genetic variation for anemotaxis (wind-directed movement) in laboratory and wild-caught populations Drosophilia. Behavior Genetics 12.
8. Yu YSW, Graff MM, and Hartmann MJZ (2016). Mechanical responses of rat vibrissae to airflow. J. Exp. Biol 219, 937–948. [PubMed: 27030774]
9. Dupuy F, Steinmann T, Pierre D, Christides JP, Cummins G, Lazzari C, Miller J, and Casas J (2012). Responses of cricket cercal interneurons to realistic naturalistic stimuli in the field. Journal of Experimental Biology 215, 2382–2389. [PubMed: 22723476]
10. Chapman JW, Klaassen RHG, Drake VA, Fossette S, Hays GC, Metcalfe JD, Reynolds AM, Reynolds DR, and Alerstam T (2011). Animal Orientation Strategies for Movement Review in Flows. CURBIO 21, R861–R870.

11. Ai H (2013). Sensors and Sensory Processing for Airborne Vibrations in Silk Moths and Honeybees. Sensors 13, 9344–9363. [PubMed: 23877129]
12. Kane EA, Gershow M, Afonso B, Larderet I, Klein M, Carter AR, de Bivort BL, Sprecher SG, and Samuel ADT (2013). Sensorimotor structure of Drosophila larva phototaxis. Proc. Natl. Acad. Sci. U.S.A. 110, E3868–77. [PubMed: 24043822]
13. Gershow M, Berck M, Mathew D, Luo L, Kane EA, Carlson JR, and Samuel ADT (2012). Controlling airborne cues to study small animal navigation. Nat. Methods 9, 290–296. [PubMed: 22245808]
14. Gepner R, Mihovilovic Skanata M, Bernat NM, Kaplow M, and Gershow M (2015). Computations underlying Drosophila photo-taxis, odor-taxis, and multi-sensory integration. eLife 4.
15. Gomez-Marin A, Duistermars BJ, Frye MA, and Louis M (2010). Mechanisms of odor-tracking: multiple sensors for enhanced perception and behavior. Front Cell Neurosci 4, 6. [PubMed: 20407585]
16. Gomez-Marin A, Stephens GJ, and Louis M (2011). Active sampling and decision making in Drosophila chemotaxis. Nat Commun 2, 441. [PubMed: 21863008]
17. Klein M, Afonso B, Vonner AJ, Hernandez-Nunez L, Berck M, Tabone CJ, Kane EA, Pieribone VA, Nitabach MN, Cardona A, et al. (2015). Sensory determinants of behavioral dynamics in Drosophila thermotaxis. Proc. Natl. Acad. Sci. U.S.A. 112, E220–9. [PubMed: 25550513]
18. Klein M, Krivov SV, Ferrer AJ, Luo L, Samuel AD, and Karplus M (2017). Exploratory search during directed navigation in C. elegans and Drosophila larva. eLife 6, e30503–14. [PubMed: 29083306]
19. Lahiri S, Shen K, Klein M, Tang A, Kane E, Gershow M, Garrity P, and Samuel ADT (2011). Two alternating motor programs drive navigation in Drosophila larva. PLoS ONE 6, e23180. [PubMed: 21858019]
20. Luo L, Gershow M, Rosenzweig M, Kang K, Fang-Yen C, Garrity PA, and Samuel ADT (2010). Navigational decision making in Drosophila thermotaxis. J. Neurosci 30, 4261–4272. [PubMed: 20335462]
21. Fishilevich E, Domingos AI, Asahina K, Naef F, Vosshall LB, and Louis M (2005). Chemotaxis behavior mediated by single larval olfactory neurons in Drosophila. CURBIO 15, 2086–2096.
22. Louis M, Huber T, Benton R, Sakmar TP, and Vosshall LB (2008). Bilateral olfactory sensory input enhances chemotaxis behavior. Nat Neurosci 11, 187–199. [PubMed: 18157126]
23. Schulze A, Gomez-Marin A, Rajendran VG, Lott G, Musy M, Ahammad P, Deogade A, Sharpe J, Riedl J, Jarriault D, et al. (2015). Dynamical feature extraction at the sensory periphery guides chemotaxis. eLife 4, 1129.
24. Kohsaka H, Guertin PA, and Nose A (2017). Neural Circuits Underlying Fly Larval Locomotion. Curr. Pharm. Des 23, 1722–1733. [PubMed: 27928962]
25. Gong Z, Liu J, Guo C, Zhou Y, Teng Y, and Liu L (2010). Two pairs of neurons in the central brain control Drosophila innate light preference. Science 330, 499–502. [PubMed: 20966250]
26. Sprecher SG, Cardona A, and Hartenstein V (2011). The Drosophila larval visual system: high-resolution analysis of a simple visual neuropil. Dev. Biol 358, 33–43. [PubMed: 21781960]
27. Slater G, Levy P, Chan KLA, and Larsen C (2015). A central neural pathway controlling odor tracking in Drosophila. J. Neurosci 35, 1831–1848. [PubMed: 25653345]
28. Tastekin I, Riedl J, Schilling-Kurz V, Gomez-Marin A, Truman JW, and Louis M (2015). Role of the subesophageal zone in sensorimotor control of orientation in Drosophila larva. Curr. Biol 25, 1448–1460. [PubMed: 25959970]
29. Flugge C (1934). Geruchliche Raumorientierung von Drosophila melanogaster.
30. Gomez-Marin A, and Louis M (2014). Multilevel control of run orientation in Drosophila larval chemotaxis. Front. Behav. Neurosci 8, 38. [PubMed: 24592220]
31. Ohyama T, Jovanic T, Denisov G, Dang TC, Hoffmann D, Kerr RA, and Zlatic M (2013). High-Throughput Analysis of Stimulus-Evoked Behaviors in Drosophila Larva Reveals Multiple Modality-Specific Escape Strategies. PLoS ONE 8, e71706. [PubMed: 23977118]
32. Jovanic T, Schneider-Mizell CM, Shao M, Masson J-B, Denisov G, Fetter RD, Mensh BD, Truman JW, Cardona A, and Zlatic M (2016). Competitive Disinhibition Mediates Behavioral Choice and Sequences in Drosophila. Cell 167, 858–870.e19. [PubMed: 27720450]

33. Jovanic T, Masson J-B, Truman JW, and Zlatic M (2017). Mapping neurons and brain regions underlying sensorimotor decisions and sequences in Drosophila. bioRxiv, 1–22.
34. Sweeney ST, Broadie K, Keane J, Niemann H, and O'Kane CJ (1995). Targeted expression of tetanus toxin light chain in Drosophila specifically eliminates synaptic transmission and causes behavioral defects. Neuron 14, 341–351. [PubMed: 7857643]
35. Fushiki A, Kohsaka H, and Nose A (2013). Role of sensory experience in functional development of Drosophila motor circuits. PLoS ONE 8, e62199. [PubMed: 23620812]
36. Tsubouchi A, Caldwell JC, and Tracey WD (2012). Dendritic filopodia, Ripped Pocket, NOMPC, and NMDARs contribute to the sense of touch in Drosophila larvae. Curr. Biol 22, 2124–2134. [PubMed: 23103192]
37. Yan Z, Zhang W, He Y, Gorczyca D, Xiang Y, Cheng LE, Meltzer S, Jan LY, and Jan Y-N (2013). Drosophila NOMPC is a mechanotransduction channel subunit for gentle-touch sensation. Nature 493, 221–225. [PubMed: 23222543]
38. Ohyama T, Schneider-Mizell CM, Fetter RD, Aleman JV, Franconville R, Rivera-Alba M, Mensh BD, Branson KM, Simpson JH, Truman JW, et al. (2015). A multilevel multimodal circuit enhances action selection in Drosophila. Nature 520, 633–639. [PubMed: 25896325]
39. McMeniman CJ, Corfas RA, Matthews BJ, Ritchie SA, and Vosshall LB (2014). Multimodal integration of carbon dioxide and other sensory cues drives mosquito attraction to humans. Cell 156, 1060–1071. [PubMed: 24581501]
40. van Atteveldt N, Murray MM, Thut G, and Schroeder CE (2014). Multisensory integration: flexible use of general operations. Neuron 81, 1240–1253. [PubMed: 24656248]
41. Fetsch CR, DeAngelis GC, and Angelaki DE (2013). Bridging the gap between theories of sensory cue integration and the physiology of multisensory neurons. Nat Rev Neurosci 14, 429–442. [PubMed: 23686172]
42. Zhang W, Yan Z, Jan LY, and Jan Y-N (2013). Sound response mediated by the TRP channels NOMPC, NANCHUNG, and INACTIVE in chordotonal organs of Drosophila larvae. Proc. Natl. Acad. Sci. U.S.A. 110, 13612–13617. [PubMed: 23898199]
43. Tsubouchi A, Caldwell JC, and Tracey WD (2012). Dendritic Filopodia, Ripped Pocket, NOMPC, and NMDARs Contribute to the Sense of Touch in Drosophila Larvae. CURBIO 22, 2124–2134.
44. Schneider-Mizell CM, Gerhard S, Longair M, Kazimiers T, Li F, Zwart MF, Champion A, Midgley FM, Fetter RD, Saalfeld S, et al. (2016). Quantitative neuroanatomy for connectomics in Drosophila. eLife 5, 1133.
45. Nern A, Pfeiffer BD, and Rubin GM (2015). Optimized tools for multicolor stochastic labeling reveal diverse stereotyped cell arrangements in the fly visual system. Proc. Natl. Acad. Sci. U.S.A. 112, E2967–76. [PubMed: 25964354]
46. Burgos A, Honjo K, Ohyama T, Qian CS, Shin GJ-E, Gohl DM, Silies M, Tracey WD, Zlatic M, Cardona A, et al. (2018). Nociceptive interneurons control modular motor pathways to promote escape behavior in Drosophila. eLife 7, 1557.
47. Rohwedder A, Wenz NL, Stehle B, Huser A, Yamagata N, Zlatic M, Truman JW, Tanimoto H, Saumweber T, Gerber B, et al. (2016). Four Individually Identified Paired Dopamine Neurons Signal Reward in Larval Drosophila. Curr. Biol 26, 661–669. [PubMed: 26877086]
48. Eichler K, Li F, Litwin-Kumar A, Park Y, Andrade I, Schneider-Mizell CM, Saumweber T, Huser A, Eschbach C, Gerber B, et al. (2017). The complete connectome of a learning and memory centre in an insect brain. Nature 548, 175–182. [PubMed: 28796202]
49. Bodmer R, and Jan Y-N (1987). Morphological differentiation of the embryonic peripheral neurons in Drosophila. Rouxs Arch. Dev. Biol 196, 69–77.
50. Merritt DJ, and Whitington PM (1995). Central projections of sensory neurons in the Drosophila embryo correlate with sensory modality, soma position, and proneural gene function. J. Neurosci 15, 1755–1767. [PubMed: 7891133]
51. Saumweber T, Rohwedder A, Schleyer M, Eichler K, Chen Y-C, Aso Y, Cardona A, Eschbach C, Kobler O, Voigt A, et al. (2018). Functional architecture of reward learning in mushroom body extrinsic neurons of larval Drosophila. Nat Commun 9, 1104. [PubMed: 29549237]
52. Cohn R, Morantte I, and Ruta V (2015). Coordinated and Compartmentalized Neuromodulation Shapes Sensory Processing in Drosophila. Cell 163, 1742–1755. [PubMed: 26687359]

53. Cognigni P, Felsenberg J, and Waddell S (2018). Do the right thing: neural network mechanisms of memory formation, expression and update in Drosophila. Current Opinion in Neurobiology 49, 51–58. [PubMed: 29258011]
54. da Silva JA, Tecuapetla F, Paixão V, and Costa RM (2018). Dopamine neuron activity before action initiation gates and invigorates future movements. Nature 79, 368.
55. Watabe-Uchida M, Eshel N, and Uchida N (2017). Neural Circuitry of Reward Prediction Error. Annu. Rev. Neurosci 40, 373–394. [PubMed: 28441114]
56. Schultz W (2015). Neuronal Reward and Decision Signals: From Theories to Data. Physiol. Rev 95, 853–951. [PubMed: 26109341]
57. Panigrahi B, Martin KA, Li Y, Graves AR, Vollmer A, Olson L, Mensh BD, Karpova AY, and Dudman JT (2015). Dopamine Is Required for the Neural Representation and Control of Movement Vigor. Cell 162, 1418–1430. [PubMed: 26359992]
58. Lewis LPC, Siju KP, Aso Y, Friedrich AB, Bulteel AJB, Rubin GM, and Grunwald Kadow IC (2015). A Higher Brain Circuit for Immediate Integration of Conflicting Sensory Information in Drosophila. Curr. Biol 25, 2203–2214. [PubMed: 26299514]
59. Fushiki A, Zwart MF, Kohsaka H, Fetter RD, Cardona A, Nose A, and Griffith LC (2016). A circuit mechanism for the propagation of waves of muscle contraction in Drosophila. eLife 5, e13253. [PubMed: 26880545]
60. Berck ME, Khandelwal A, Claus L, Hernandez-Nunez L, Si G, Tabone CJ, Li F, Truman JW, Fetter RD, Louis M, et al. (2016). The wiring diagram of a glomerular olfactory system.
61. Schlegel P, Texada MJ, Miroschnikow A, Schoofs A, Hückesfeld S, Peters M, Schneider-Mizell CM, Lacin H, Li F, Fetter RD, et al. (2016). Synaptic transmission parallels neuromodulation in a central food-intake circuit. eLife 5, 462.
62. Zwart MF, Pulver SR, Truman JW, Fushiki A, Fetter RD, Cardona A, and Landgraf M (2016). Selective Inhibition Mediates the Sequential Recruitment of Motor Pools. Neuron 91, 615–628. [PubMed: 27427461]
63. Larderet I, Fritsch PM, Gendre N, Neagu-Maier GL, Fetter RD, Schneider-Mizell CM, Truman JW, Zlatic M, Cardona A, and Sprecher SG (2017). Organization of the Drosophila larval visual circuit. eLife 6, e28387–23. [PubMed: 30726702]
64. Karagyozov D, Mihovilovic Skanata M, Lesar A, and Gershow M (2017). Recording neural activity in unrestrained animals with 3D tracking two photon microscopy. bioRxiv, 1–34.
65. Pfeiffer BD, Jenett A, Hammonds AS, Ngo T-TB, Misra S, Murphy C, Scully A, Carlson JW, Wan KH, Laverty TR, et al. (2008). Tools for neuroanatomy and neurogenetics in Drosophila. Proc. Natl. Acad. Sci. U.S.A. 105, 9715–9720. [PubMed: 18621688]
66. Pfeiffer BD, Ngo T-TB, Hibbard KL, Murphy C, Jenett A, Truman JW, and Rubin GM (2010). Refinement of tools for targeted gene expression in Drosophila. Genetics 186, 735–755. [PubMed: 20697123]
67. Swierczek NA, Giles AC, Rankin CH, and Kerr RA (2011). High-throughput behavioral analysis in C. elegans. Nat. Methods 8, 592–598. [PubMed: 21642964]
68. Saalfeld S, Cardona A, Hartenstein V, and Tomancak P (2009). CATMAID: collaborative annotation toolkit for massive amounts of image data. Bioinformatics 25, 1984–1986. [PubMed: 19376822]
69. Jenett A, Rubin GM, Ngo T-TB, Shepherd D, Murphy C, Dionne H, Pfeiffer BD, Cavallaro A, Hall D, Jeter J, et al. (2012). A GAL4-Driver Line Resource for Drosophila Neurobiology. Cell Rep 2, 991–1001. [PubMed: 23063364]
70. Zhou B, Hofmann D, Pinkoviezky I, Sober SJ, and Nemenman I (2018). Chance, long tails, and inference in a non-Gaussian, Bayesian theory of vocal learning in songbirds. Proc. Natl. Acad. Sci. U.S.A. 115, E8538–E8546. [PubMed: 30127024]

Highlights

1. *Drosophila* larvae perform negative anemotaxis
2. To anemotax, larvae modulate the turn rate, size and direction as in other taxes
3. Chordotonal and multidendritic class III sensory neurons together mediate anemotaxis
4. The anemotactic circuitry involves both the nerve cord and the brain

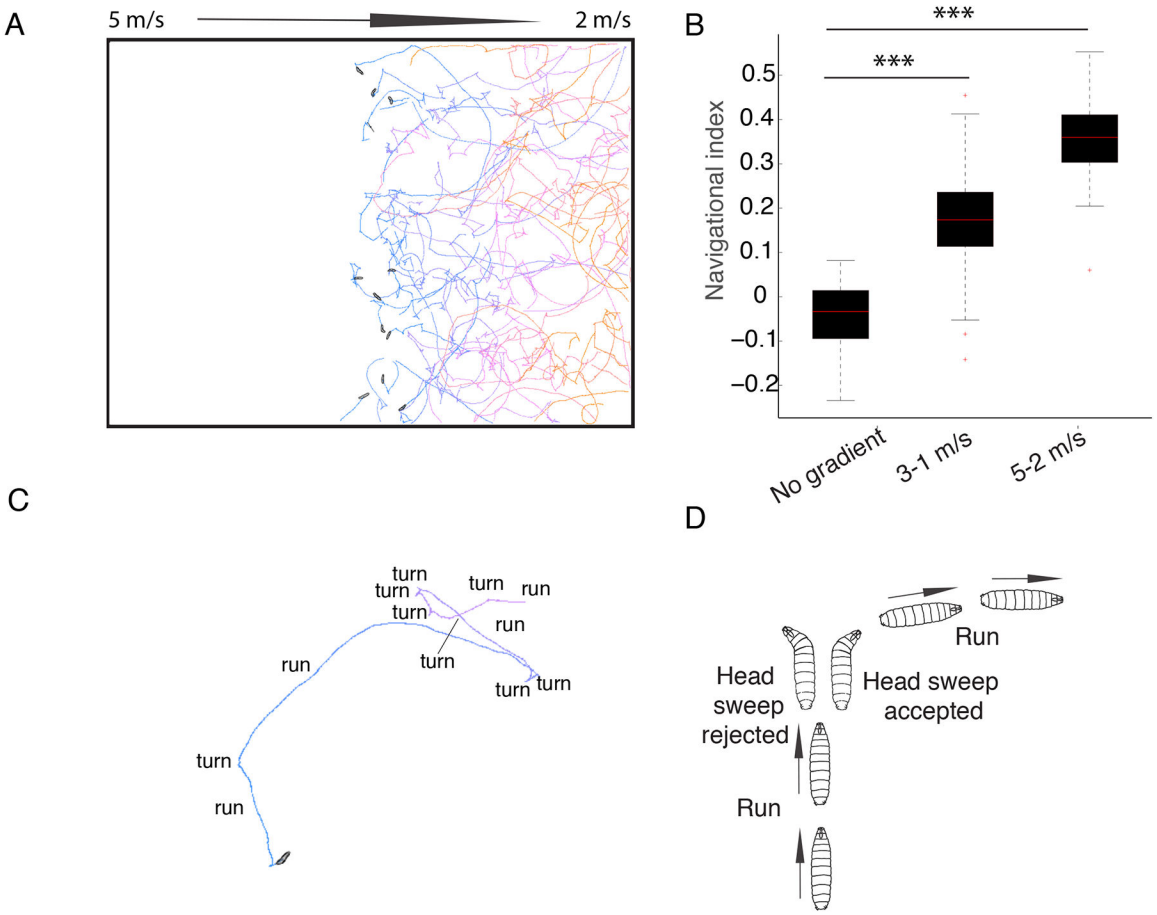

Figure 1. Drosophila Larvae perform negative anemotaxis.

A. In air-speed gradients, the larvae navigate down the gradient. The colors of the tracks represent the time from the beginning of the experiment (blue) to the end (orange). Snapshots of the initial positions of larvae in the center of the agar plate are shown B. Navigational index in 3–1 m/s and 5–2 m/s gradient compared to no-gradient conditions. In the box plot the median is indicated by the red horizontal line. Box boundaries represent first and third quartiles, whiskers extend to the most extreme data points not considered outliers. The outliers are indicated by red + C. Larvae alternate periods of runs and turns D. An example of a reorientation event where a larva perpendicular to the direction of the gradient accepts a head sweep and extends a run in a favorable direction is shown. P-values and N of animals are shown in Data S1 and Table S2, respectively).

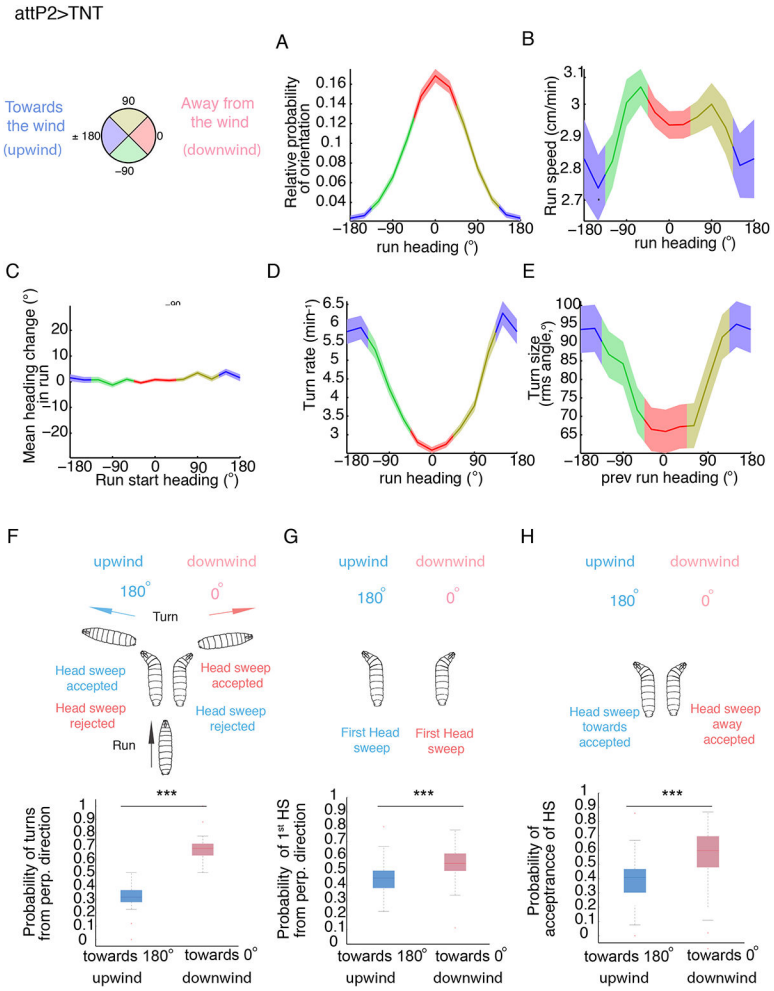

Figure 2. Behavioral strategies of Drosophila larvae during anemotaxis.

Behavioral strategies in anemotaxis in control *attP2> TNT* (the same is shown for *attP2-attP40> TNT* in Figure S1). A compass in which 0° indicates the direction down the gradient (downwind) and 180° up the gradient (upwind) was used to keep track of larval direction during runs and turns as a function of the wind-speed spatial gradient.

A. Relative probability of headings during runs. B. Speed versus heading during runs C. Mean heading change in runs D. Turn rate versus heading E. Turn size versus heading F. Distribution of turns from perpendicular direction G. Distribution of head sweeps from perpendicular direction H. Probability of starting a run during a head sweep A-E Values are mean and s.e.m. F-H. In the box plot the median is indicated by the horizontal line. Box boundaries represent first and third quartiles, whiskers extend to the most extreme data points not considered outliers. The outliers are indicated by red +. *: $p<0.05$, **: $p<0.01$, ***:$<p<0.001$ (p-values can be found in Data S1 and the N of animals in Table S2). See also Figure S1 and Data S3.

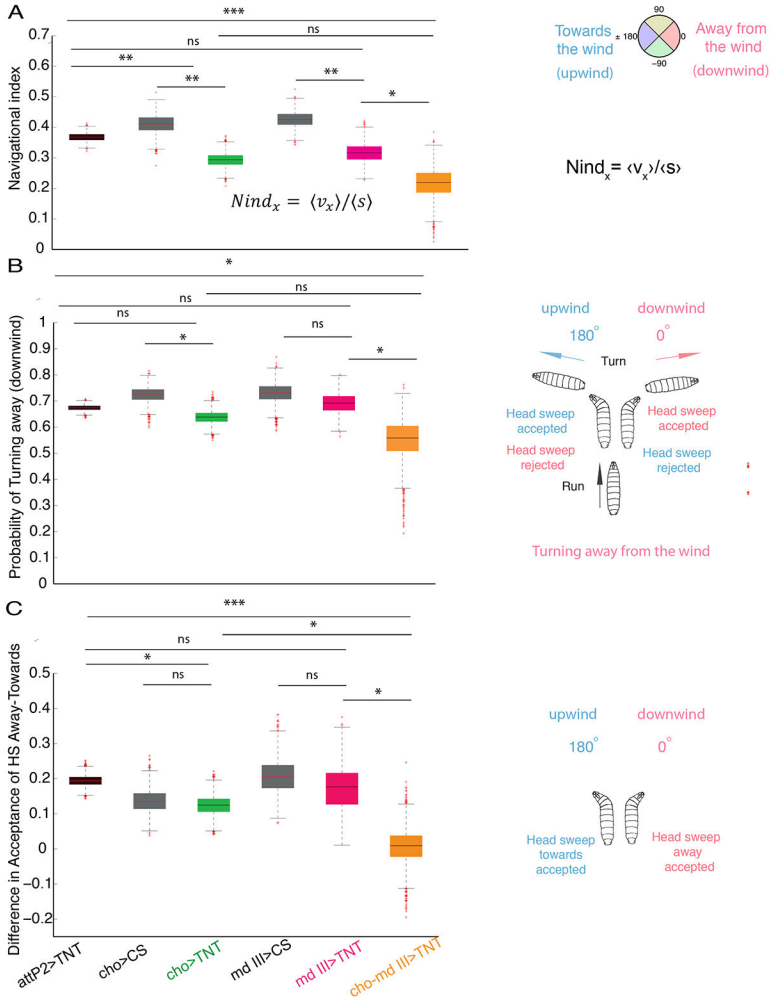

Figure 3. Somatosensory neurons implicated in anemotaxis.

A. Comparison of the navigation index in chordotonal>TNT (*cho> TNT*), multidendritic class III>TNT (*md III> TNT*), chordotonal-multidendritic class III>TNT (*cho-md III> TNT*) and control larvae. Silencing of cho and md III neurons simultaneously impairs anemotaxis. B. Probability of turns from perpendicular direction away from the wind (downwind) (0°) in *cho> TNT*, *md III> TNT* and *cho-md III> TNT*. Larvae with silenced cho and md III neurons together have a lower probability of turning away from the wind than the control and *md III> TNT* larvae C. Differences in probabilities of starting a run during a head sweep from perpendicular direction away and towards the wind. Larvae with silenced cho and md III neurons together have a lower difference in acceptance of head sweep away from and towards the wind compared to larvae with silenced md III and cho individually as well as control *attP2> TNT* larvae. Bootstrapped values are shown. In the box plot the median is indicated by the horizontal line. Box boundaries represent first and third quartiles, whiskers extend to the most extreme data points not considered outliers. The outliers are indicated by red +. *: p<0.05, **: p<0.01, ***:<p<0.001 (p-values can be found in Data S1 and S4, the N of animals in Table S2). See also Figure S2 and Data S2

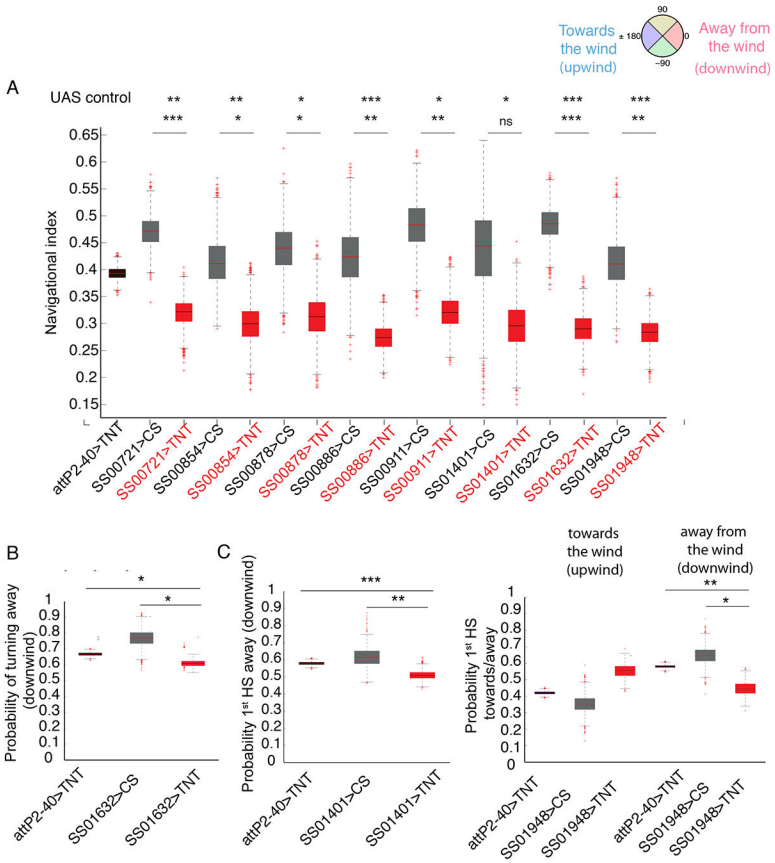

Figure 4. Identifying central neurons whose silencing leads to reduced performance in anemotaxis.

A. Navigational indices of eight lines with less efficient anemotaxis compared to respective GAL4 controls and *attP2-attP40>TNT* control. Bootstrapped values are shown. *: p<0.05, **: p<0.01, ***:<p<0.001 (p-values can be found in Data S1). B. Probability of turns from perpendicular direction away from the wind (downwind) (0°) in *SS01632>TNT* compared to the controls *attP2-attP40>TNT* and *SS01632>CS* C. Probability of first head sweep from perpendicular direction away from the wind (downwind) (0°) in *SS01401>TNT* and *SS01948>TNT* compared to the control *attP2-attP40>TNT* Bootstrapped values are shown. In the box plot the median is indicated by the red horizontal line. Box boundaries represent first and third quartiles, whiskers extend to the most extreme data points not considered outliers. The outliers are indicated by red +. *: p<0.05, **: p<0.01, ***: <p<0.001 (p-values can be found in Data S1 and S4, the N of animals in Table S2). See also Figures S3, S4, Table S1 and Data S2

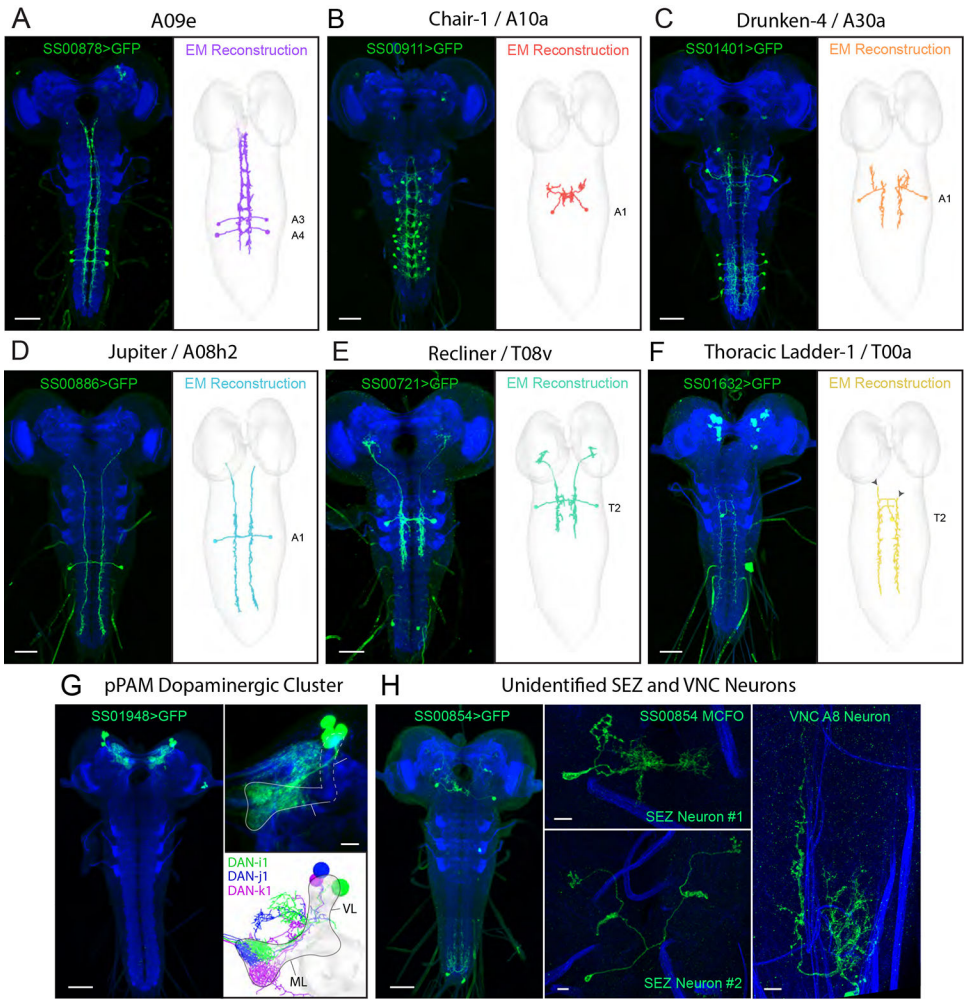

Figure 5. Electron microscopy correlates and connectivity of first-order anemotaxis neurons.

(A-F) Light microscopy z-projections of Split-GAL4s driving GFP expression in L3 (*left panels*) and the corresponding neuron reconstructed in a ssTEM L1 volume (*right panels*). A-C depict previously reconstructed neurons that have now been matched with Split-GAL4 lines. D-F depict neurons identified in EM and reconstructed for this study. Solid arrowheads indicate the ends of dendritic branches for comparison between light and EM images. Double arrowheads indicate contaminant neurons. (G) Expression pattern of *SS01948* driving GFP expression in L3 (*left panel*). This line expresses in the pPAM cluster of four dopaminergic neurons that tile the mushroom body medial lobe (*right panel*). Note that four cell bodies are present, but only three DANs are presented in EM (DAN-h1 is not present in the ssTEM L1 volume and thus cannot be directly compared). (H) Expression pattern of *SS00854* driving GFP expression in L3, depicting multiple neurons (*left panel*). MCFO revealed two SEZ neurons (*middle panels*) and an A8 VNC neuron (*right panel*). Scale bars are 50 μm unless indicated as 10 μm. See also Figure S5 and Data S5.

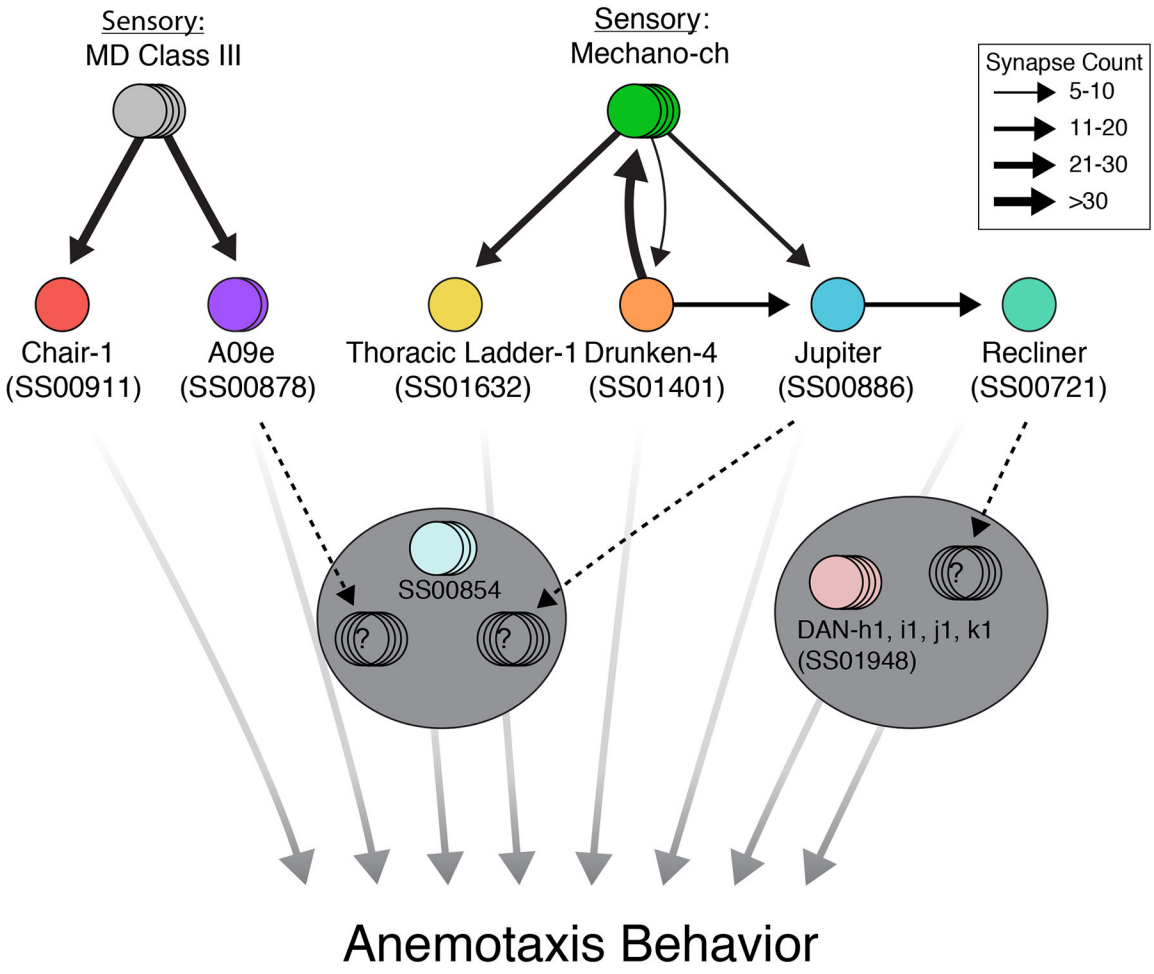

Figure 6. Anemotaxis circuit.

Chair-1 and A09e receive strong inputs from md III neurons, while Thoracic Ladder-1, Drunken-4, and Jupiter receive inputs from cho neurons. A second-order mechanosensory neuron, Recliner, was also identified downstream of Jupiter. Note that although no direct convergence between md III and cho neurons is reported here, two first-order neurons project to the SEZ (A09e and Jupiter) and the second-order Recliner projects to the brain at potential convergence sites (see dashed black arrows). No EM correlate has yet been found for *SS00854*. Width of black arrows indicates synaptic strength. All neurons reported here are involved in anemotaxis. See also Data S5